Article

SOURCE DATA | TRANSPARENT PROCESS

EMBO reports

HP1 maintains protein stability of H3K9 methyltransferases and demethylases

Ryo Maeda[1,2] & Makoto Tachibana[1,2,*]

Abstract

Di- or tri-methylated H3K9 (H3K9me2/3) is an epigenetic mark of heterochromatin. Heterochromatin protein 1 (HP1) specifically recognizes H3K9me2/3, contributing to transcriptional suppression and spread of H3K9me2/3. Here, we demonstrate another role of HP1 in heterochromatin organization: regulation of protein stability of H3K9 methyltransferases (H3K9 MTs) and demethylases (H3K9 DMs). We show that HP1 interaction-defective mutants of H3K9 MTs, Suv39h1 and Setdb1, undergo protein degradation. We further establish mouse embryonic stem cell lines lacking all three HP1 paralogs. In the HP1-deficient cells, Suv39h1, Suv39h2, Setdb1, and G9a/GLP complex decrease at the protein level, and the enzymes are released from chromatin. HP1 mutants that cannot recognize H3K9me2/3 or form dimers cannot stabilize these enzymes, indicating that the tethering of H3K9 MTs to chromatin is critical for their protein stability. We show that HP1 also stabilizes H3K9 DMs, Jmjd1a and Jmjd1b. Our study indicates that mammalian HP1 forms a heterochromatin hub that governs protein stability of H3K9 MTs and H3K9 DMs.

Keywords HP1; heterochromatin; H3K9 methyltransferase; H3K9 demethylase; H3K9me2/3

Subject Categories Chromatin, Transcription & Genomics

DOI 10.15252/embr.202153581 | Received 7 July 2021 | Revised 20 January 2022 | Accepted 24 January 2022 | Published online 15 February 2022

EMBO Reports (2022) 23: e53581

Introduction

The covalent modification of histone tail regions plays a central role in regulating various nuclear events in eukaryotes (Jenuwein & Allis, 2001). Histone modification levels are regulated by the opposite mechanisms of action of modification-depositing enzymes ("writer") and modification-removing enzymes ("eraser"). The input of histone modification is recognized by "reader" proteins and is converted into specific biological outputs, such as transcription regulation (Wysocka *et al*, 2006; Margueron *et al*, 2009; Canzio *et al*, 2011).

Di- or tri-methylated H3K9 (H3K9me2/3) is preferentially enriched in gene-poor regions of chromosomes, forming transcriptionally suppressed heterochromatin (Martens *et al*, 2005; Mikkelsen *et al*, 2007; Canzio *et al*, 2011; Kuroki *et al*, 2018). Suv39h1 is the first discovered H3K9 methyltransferase (H3K9 MT) responsible for H3K9me3 in pericentric heterochromatin (Rea *et al*, 2000). Setdb1 mainly catalyzes H3K9me3 at retroelement-derived sequences (Matsui *et al*, 2010). We previously showed that G9a/GLP complex is responsible for H3K9me1/2 in a wide range of chromosomal regions (Tachibana *et al*, 2002; Tachibana *et al*, 2005). H3K9me2 catalyzed by G9a/GLP complex is antagonistically removed by two H3K9 demethylases (H3K9 DMs), Jmjd1a and its related paralog Jmjd1b (Kuroki *et al*, 2018).

Heterochromatin protein 1 (HP1) is a representative reader protein of H3K9me2/3. HP1 contains two functional domains: a chromodomain and a chromoshadow domain. The former specifically binds to H3K9me2/3 (Bannister *et al*, 2001; Lachner *et al*, 2001), and the latter is required for dimerization, which provides a binding interface for various proteins, including transcription corepressors and H3K9 MTs (Aagaard *et al*, 1999; Cowieson *et al*, 2000; Thiru *et al*, 2004; Ivanov *et al*, 2007; Nozawa *et al*, 2010). The protein–protein interaction between HP1 and H3K9 MTs is considered important for the H3K9me writing process; HP1 tethers H3K9 MTs to H3K9me2/3-containing chromatin through this interaction, thereby promoting the spreading of H3K9me2/3 into the neighboring nucleosomes (Bannister *et al*, 2001).

Here, we show another crucial role of HP1 in mammalian heterochromatin organization: HP1 regulates protein stability of H3K9 MTs. In the absence of HP1, Suv39h1/2, Setdb1, and G9a/GLP complexes were significantly reduced at the protein level. Mutant analysis of HP1 indicates that HP1 ensures protein stability of H3K9 MTs by tethering these enzymes to chromatin. Furthermore, we also found that HP1 regulates protein stability of H3K9 DMs, Jmjd1a and Jmjd1b. These results indicate that HP1 forms a robust catalytic core for H3K9 methylation and demethylation.

Results

HP1 interaction-defective Suv39h1 and Setdb1 proteins are degraded via the proteasome pathway

A previous study demonstrated that Suv39h1 directly binds to HP1 (Yamamoto & Sonoda, 2003). This study showed that the N terminus of Suv39h1 is required for HP1 interaction, and ΔN-Suv39h1,

1 Graduate School of Frontier Biosciences, Osaka University, Osaka, Japan
2 Institute of Advanced Medical Sciences, Tokushima University, Tokushima, Japan
*Corresponding author. E-mail: tachiban@fbs.osaka-u.ac.jp

which lacks 41 amino acids at the N terminus of Suv39h1, cannot bind to HP1. We previously found that ΔN-Suv39h1 still possess H3K9 methylation activity but tended to be less expressed than wild-type Suv39h1 at the protein level, even though their mRNA was expressed similarly (Muramatsu *et al*, 2016). We therefore assumed that HP1-Suv39h1 interaction might be important for protein stability of Suv39h1. Co-immunoprecipitation followed by immunoblotting confirmed that ΔN-Suv39h1 is unable to bind to HP1 (Fig 1A and B). We next established mouse embryonic stem cell (mESC) lines stably expressing ΔN-Suv39h1 and wild-type Suv39h1 and compared their protein stability. Chase analyses using the protein synthesis inhibitor cycloheximide (CHX) revealed a more rapid decay of ΔN-Suv39h1 than wild-type Suv39h1 (Fig 1C). The decayed level of ΔN-Suv39h1 protein was blocked by the 26S proteasome inhibitor, MG132, indicating that HP1 interaction-defective Suv39h1 undergoes protein degradation through the proteasome pathway.

Setdb1 is an H3K9 MT responsible for H3K9me3 at retroelements (Matsui *et al*, 2010). Other studies have found that Setdb1 indirectly associates with HP1, showing that the SUMO-interacting motif of the amino acid sequence from 122 to 125 in human SETDB1 is responsible for the HP1 interaction (Schultz *et al*, 2002; Ivanov *et al*, 2007). Despite these facts, we re-assessed the protein–protein interaction between Setdb1 and HP1. We searched for the HP1 interaction motif PXVXL in the amino acid sequence of Setdb1 and found 344PMVLL348 in the Tudor domain and 617PLLVPL622 in the MBD domain (Fig 1D). Co-immunoprecipitation followed by immunoblotting revealed that the former sequence is dispensable, but the latter sequence is required for HP1 interaction; a mutant of Setdb1 (Setdb1-3A) harboring three amino acid substitutions of 617PLLVPL622 to ALLAPA never interacted with HP1 (Fig 1E and F). We found that Setdb1 expressed in mammalian cells interacts with recombinant HP1 but that expressed in bacteria does not (Fig EV1A), suggesting indirect interaction between Setdb1 and HP1. Previous studies demonstrated that Setdb1 undergoes monoubiquitination, which is required for the enzymatic activity of Setdb1 (Ishimoto *et al*, 2016; Sun & Fang, 2016). As shown in Fig EV1B, mono-ubiquitinated form of Setdb1 was undetectable in Setdb1-3A. Furthermore, Setdb1-3A did not exhibit H3K9 methylation activity (Fig EV1C). These results indicate that 617PLLVPL622 of Setdb1 is crucial for HP1 interaction, monoubiquitination, and H3K9 methylation activity. Chase analyses indicated that HP1 interaction-defective Setdb1-3A underwent protein degradation via the proteasome pathway (Fig 1G). Collectively, these results suggest that HP1 interaction is crucial for maintaining protein stability of Suv39h1 and Setdb1.

Establishment of HP1-deficient mESCs

To confirm the importance of HP1-H3K9 MTs interaction in ensuring protein stability of H3K9 MTs, we aimed to elucidate whether HP1 depletion affects protein expression levels of H3K9 MTs. Mouse and human cells have three HP1 paralogs, HP1α, HP1β, and HP1γ, all of which recognize H3K9me2/3 and form dimers (Brasher *et al*, 2000; Cowieson *et al*, 2000; Hiragami-Hamada *et al*, 2011). We applied CRISPR/Cas-mediated genome editing for these HP1 paralogs into an mESC line, TT2. We could establish mESC lines lacking two HP1 paralogs in any combination (Fig EV2A). However, we could never establish an mESC line lacking all three HP1 paralogs, possibly indicating that complete loss of HP1 paralogs might induce growth defects. We, therefore, created conditional triple-knockout (cTKO) mESCs, in which endogenous HP1 paralogs were disrupted but maintained cellular viability by *Myc-human HP1β* (*hHP1β*) transgene (Fig 2A). In this line, the *Myc-hHP1β* transgene can be excised in the presence of 4-hydroxytamoxifen (4OHT) by Cre-loxP recombination. Immunoblot confirmed that HP1-cTKO cells did not possess endogenous HP1 paralog proteins and that exogenous Myc-hHP1β disappeared 4 days after 4OHT treatment (Fig EV2B). We next monitored the cell growth of HP1-cTKO cells in the presence of 4OHT (Fig EV2C). As expected, the number of cells increased only during the first 2 days and then decreased, indicating that mESCs could not grow without all three HP1 paralogs. On the other hand, mESCs without any two of the three HP1 paralogs were viable (Fig EV2D), indicating that at least one HP1 paralog is required for ensuring mESC viability.

HP1 regulates protein stability of Suv39h1/2, Setdb1, and G9a/GLP complex

To elucidate how HP1 depletion influences protein stability of H3K9 MTs, we measured the protein levels of H3K9 MTs in HP1-cTKO cells after 4OHT treatment. The protein levels of Suv39h1 and its

Figure 1. HP1 interaction-defective Suv39h1 and Setdb1 proteins are degraded via the proteasome pathway.

A Schematic illustration of Suv39h1 protein. ΔN-Suv39h1 lacks the 41 N-terminal amino acids but contains a chromodomain.

B Co-immunoprecipitation analysis to elucidate the interaction between Suv39h1 and HP1. Whole-cell extracts of HEK293T cells expressing 3xFlag-Suv39h1 or 3xFlag-ΔN-Suv39h1 were subjected to immunoprecipitation with the anti-Flag tag antibody followed by immunoblotting with the indicated antibodies. IgG represents the heavy- or light-chain of IgG.

C Protein decay analysis of HP1 interaction-defective Suv39h1 mutant. mESC lines stably expressing 3xFlag-Suv39h1 or 3xFlag-ΔN-Suv39h1 were treated with CHX and MG132 for the indicated times. p53 was used as the positive control for the protein decay analysis. Stacked bar plots show the summarized protein amounts of Suv39h1 (bottom). Data represented as mean ± SD ($n = 4$, biological replicates). $^{**}P < 0.01$ (Tukey's honestly significant difference test).

D Schematic illustration of Setdb1 protein with putative HP1-binding motifs. Setdb1-5A and Setdb1-3A carry substitutions of amino acids from 344PMVLL348 to AMALA and from 617PLLVPL622 to ALLAPA, respectively.

E, F Co-immunoprecipitation analysis to elucidate the interaction between Setdb1 and HP1. Whole-cell extracts of HEK293T cells expressing 3xFlag-Setdb1 or 3xFlag-Setdb1 mutants were subjected to immunoprecipitation with the anti-Flag tag antibody (E) or the anti-HP1β antibody (F). The immunocomplex was analyzed by immunoblotting with the indicated antibodies.

G Protein decay analysis of HP1 interaction-defective Setdb1 mutant. mESC lines stably expressing 3xFlag-Setdb1 or 3xFlag-Setdb1-3A were treated with CHX and MG132 for the indicated times. Stacked bar plots show the summarized protein amounts of Setdb1 (right).

Data information: Data represented as mean ± SD ($n = 4$, biological replicates). $^{**}P < 0.01$ (Tukey's honestly significant difference test).

Source data are available online for this figure.

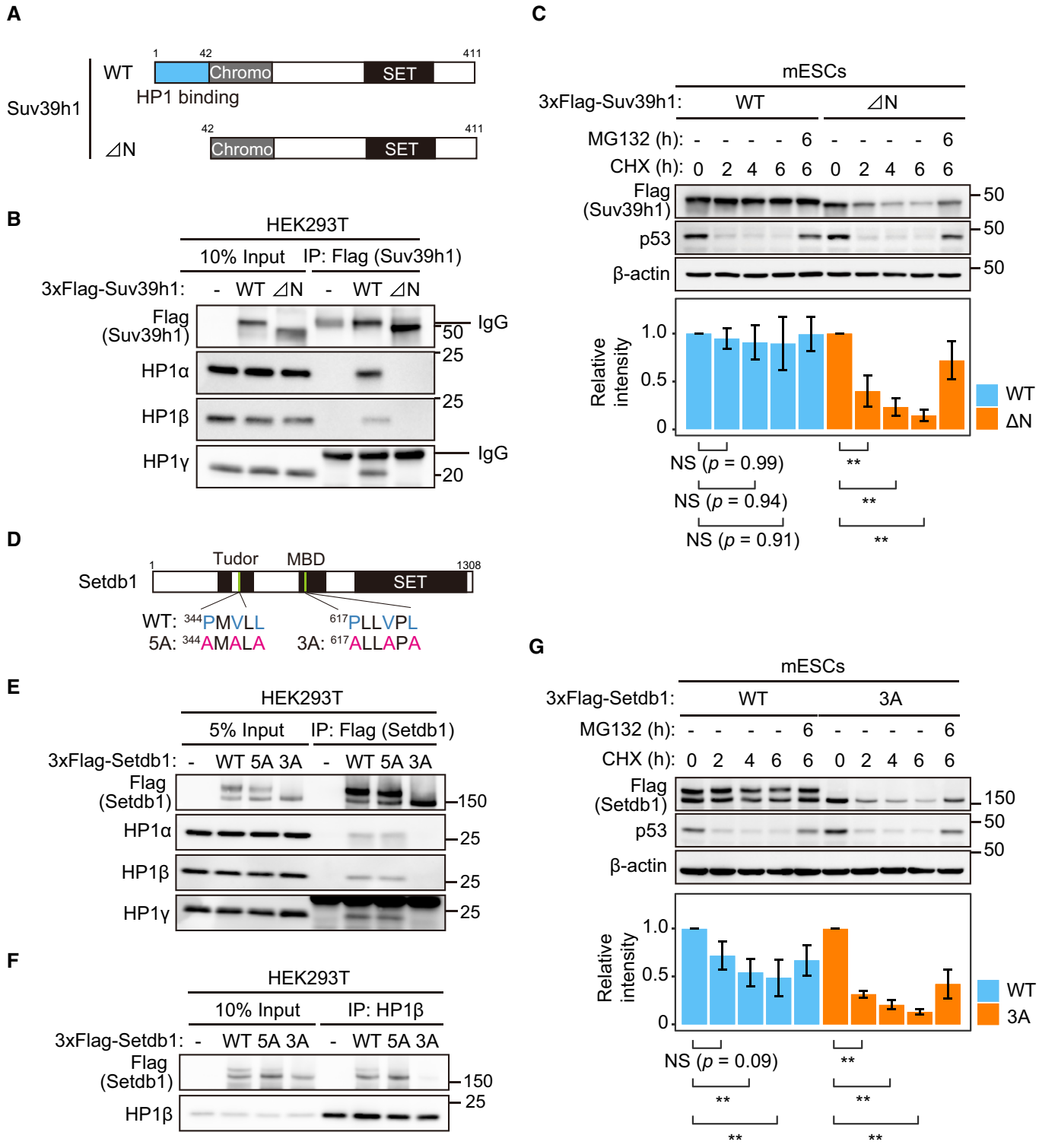

Figure 1.

closely related paralog, Suv39h2 (O'Carroll *et al*, 2000), decayed concomitantly with the decrease of Myc-HP1β (Fig 2B). Setdb1 protein also decayed with similar kinetics. We next examined the protein levels of G9a/GLP complex and found that they similarly decayed in the absence of HP1. In contrast to H3K9 MTs, the protein expression level of an H3K27MT Ezh2 was essentially unchanged, indicating that protein decay in HP1-depleted cells occurs specifically in H3K9 MTs. Quantified protein levels of Suv39h1, Suv39h2, Setdb1, G9a, and GLP were reduced to 17, 7, 31, 21, and 23%, respectively, in HP1-cTKO cells 4 days after 4OHT treatment. We

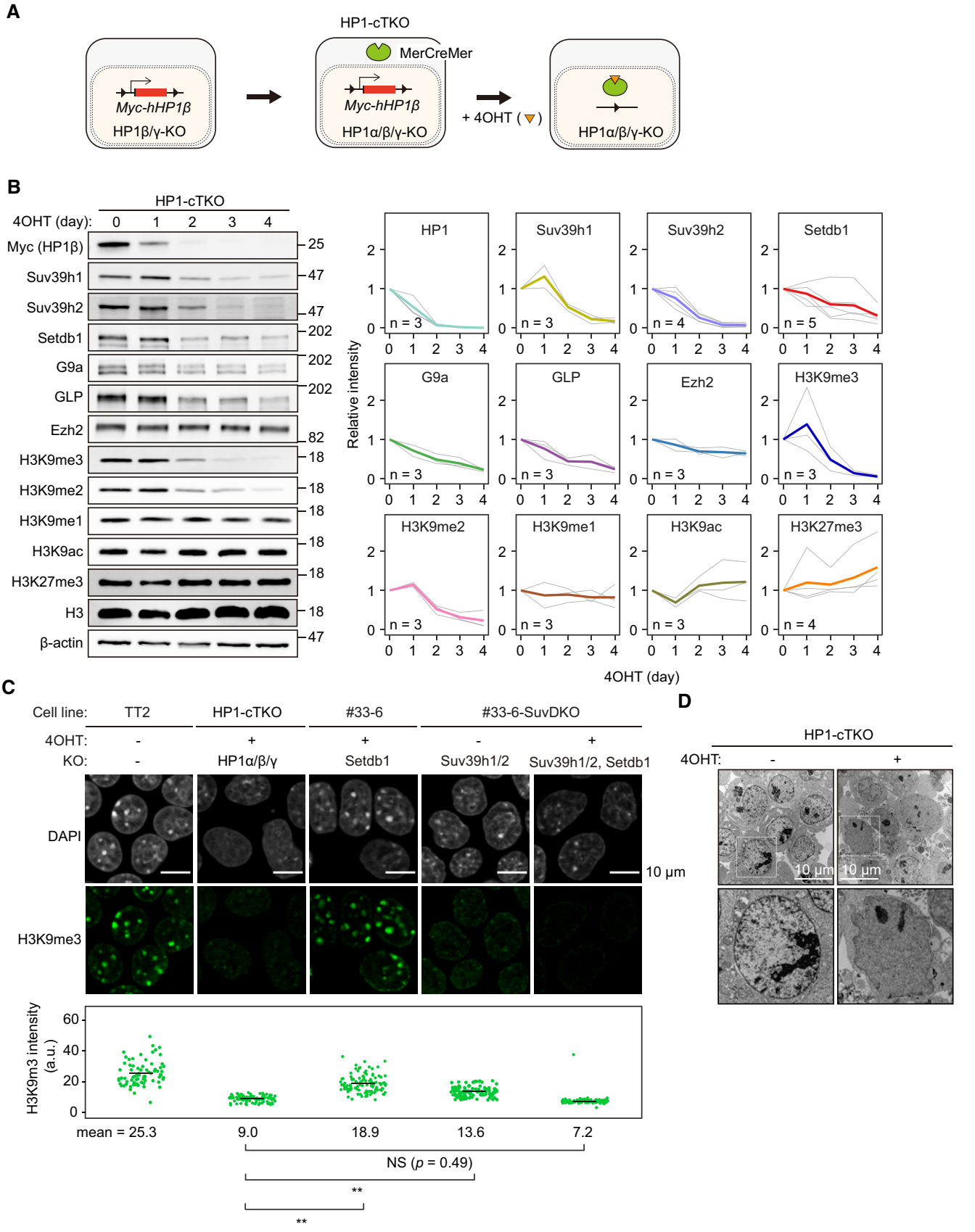

Figure 2.

Figure 2. HP1 regulates protein stability of Suv39h1/2, Setdb1, and G9a/GLP complex.

A Strategies to establish HP1 conditional triple-KO mESC lines named HP1-cTKO. After the disruption of HP1β/γ by CRISPR/Cas, an expression construct of loxP-flanked Myc-hHP1β was introduced into an mESC line, TT2. Next, we disrupted the HP1α allele by CRISPR/Cas and subsequently introduced an expression construct for mER and Cre fusion protein (MerCreMer). When HP1-cTKO cells are cultured in the presence of 4OHT, *Myc-hHP1β* transgene can be removed by Cre-loxP recombination, thereby generating mESCs that lack HP1 completely.

B Protein expression levels of H3K9 MTs and histone modification levels in HP1-cTKO cells were monitored by immunoblotting. The intensities were quantified using ImageJ software and summarized on the right. The thin gray line and bold colored line show individual data and means of the experimental replicates ($n \geq 3$, biological replicates), respectively.

C Comparison of H3K9me3 levels between HP1-deficient cells and Suv39h/Setdb1-deficient cells. The establishment of #33-6-SuvDKO is described in Fig S2. H3K9me levels were quantified using ImageJ software and summarized at the bottom; the horizontal line represents the mean intensity of each cell. More than 75 nuclei were counted for each staining. $^{**}P < 0.01$ (Tukey's honestly significant difference test).

D Electron microscopy images of HP1-cTKO cells in the absence of 4OHT (left) and the cells treated with 4OHT for 4 days (right). Boxes represent enlarged images.

Source data are available online for this figure.

Table 1. Mutated alleles for HP1-DKO and HP1-cTKO mESCs.

Line	Target	Allele	Sequence	Mutation
HP1β/γ-DKO clone GB12	*HP1β*	WT allele	GTTTGGAGCCAGAGCGGATTATTGGAGCTACTGACT	–
		KO allele1	GTTTGGAGCCAGAGC----------TACTGACT	−13 bp
		KO allele2	GTTTGGAGCCAGAGC----------TACTGACT	−13 bp
	HP1γ	WT allele	TACTGGACCGTCGTGTAGTGAATGGGAAGGTGGAGT	–
		KO allele1	TACTGGACCGTCGTGTAGT--ATGGGAAGGTGGAGT	−2 bp
		KO allele2	TACTGGACCGTCGTGTAG----------GTGGAGT	−11 bp
HP1α/γ-DKO clone GA6	*HP1α*	WT allele	AGCAAAGCAATGATATCGCTCGGGGCTTTGAGAGAG	
		KO allele1	AGCAAAGCAATGATATCG----GGGCTTTGAGAGAG	−4 bp
		KO allele2	AGCAAAGCAATGATATCGCCTCGGGGCTTTGAGAGA	+1 bp
	HP1γ	WT allele	TACTGGACCGTCGTGTAGTGAATGGGAAGGTGGAGT	–
		KO allele1	TACTGGACCGTCGTGTAGT--ATGGGAAGGTGGAGT	−2 bp
		KO allele2	TACTGGACCGTCGTGTAG----------GTGGAGT	−11 bp
HP1α/β-DKO clone BA3	*HP1α*	WT allele	AGCAAAGCAATGATATCGCTCGGGGCTTTGAGAGAG	–
		KO allele1	AGCAAAGCAATGATATCG----GGGCTTTGAGAGAG	−4 bp
		KO allele2	AGCAAAGCAATGATATCG-------CTTTGAGAGAG	−7 bp
	HP1β	WT allele	GTTTGGAGCCAGAGCGGATTATTGGAGCTACTGACT	–
		KO allele1	GTTTGGAGCCAGAGC----------TACTGACT	−13 bp
		KO allele2	GTTTGGAGCCAGAGC----------TACTGACT	−13 bp
HP1-cTKO clone A6	*HP1α*	WT allele	AGCAAAGCAATGATATCGCTCGGGGCTTTGAGAGAG	–
		KO allele1	AGCAAAGCAATGATATCG-TCGGGGCTTTGAGAGAG	−1 bp
		KO allele2	AGCAAAGCAATGATATCG-TCGGGGCTTTGAGAGAG	−1 bp
	HP1β	WT allele	GTTTGGAGCCAGAGCGGATTATTGGAGCTACTGACT	–
		KO allele1	GTTTGGAGCCAGAGC----------TACTGACT	−13 bp
		KO allele2	GTTTGGAGCCAGAGC----------TACTGACT	−13 bp
	HP1γ	WT allele	TACTGGACCGTCGTGTAGTGAATGGGAAGGTGGAGT	–
		KO allele1	TACTGGACCGTCGTGTAGT--ATGGGAAGGTGGAGT	−2 bp
		KO allele2	TACTGGACCGTCGTGTAG----------GTGGAGT	−11 bp

Underlines in WT alleles represent the PAM sequence.

simultaneously monitored H3K9me levels in HP1-cTKO cells, revealing that H3K9me3 and H3K9me2 decreased concomitantly with the decay of H3K9 MT proteins (Fig 2B). In contrast, the modification levels of H3K9me1, H3K9ac, and H3K27me3 were essentially unchanged following HP1 depletion. To examine the functional redundancy between the HP1 paralogs, we established HP1-cTKO cells carrying an additional transgene of Flag-tagged HP1 (Fig EV2E). Protein stability of H3K9MTs was maintained in cTKO cells expressing any one of the HP1 paralogs even after 4OHT treatment, confirming that all HP1 paralogs exhibit the ability to ensure protein stability of H3K9MTs. Intriguingly, the ability of HP1α to stabilize Suv39h1 is partial.

To address the cause of reduced H3K9 MT proteins, we examined those mRNA expression levels in HP1-cTKO cells after 4OHT

treatment. RT-qPCR indicated that the mRNA expression levels of *Suv39h1/2* and *Setdb1* were not decreased by HP1 depletion (Fig EV2F), confirming that Suv39h1/2 and Setdb1 decay at the protein level. We found that the mRNA levels of G9a and GLP were, respectively, reduced to approximately 50 and 75% in HP1-cTKO cells, 4 days after 4OHT treatment. However, as shown in Fig 2B, the decreased levels of G9a/GLP proteins were more prominent than those of *G9a/GLP* mRNAs, indicating that G9a/GLP complex also undergoes protein destabilization in the absence of HP1.

The present findings strongly suggest that reduced H3K9me2/3 in HP1-deficient cells is caused by the massive decay of H3K9 MT proteins. To evaluate this notion, we established an mESC line (#33-6-SuvDKO) lacking H3K9 tri-methyltransferases, Suv39h1/2 and Setdb1 (Fig EV3A), and compared their H3K9me3 levels with those in HP1-depleted cells (Fig 2C). As expected, H3K9me3 levels in HP1-deficient mESCs were comparable to those in mESCs lacking Suv39h1/2 and Setdb1. These results indicate that HP1 depletion phenocopies Suv39h/Setdb1 depletion in terms of H3K9me3 hypomethylation.

A previous study showed that Suv39h1 regulates protein stability of HP1 in mouse fibroblast (Raurell-Vila *et al*, 2017). However, in mESCs, protein expression level of HP1β in #33-6-SuvDKO cells was comparable to that in wild-type cells (Fig EV3B), indicating that HP1 regulates protein stability of H3K9 MTs but not *vice versa*. To further address this, protein expression of HP1 in H3K9 MTs-deficient mESCs was examined by immunofluorescence (Fig EV3C). Although nuclear distributions of HP1 were altered by the loss of H3K9 MTs, HP1 intensities in the whole nucleus were almost unchanged by the loss of H3K9 MTs. Thus, it is likely that H3K9 MTs might not regulate protein stability of HP1 in mESCs.

Next, we used scanning electron microscopy to examine how the depletion of HP1 and the resulting loss of H3K9 MT proteins influence nuclear architecture (Fig 2D). We referred to HP1-cTKO cell nuclei before and after 4OHT treatment as control nuclei and HP1-depleted nuclei, respectively. Control nuclei exhibited a typical smooth oval shape. In contrast, HP1-depleted nuclei exhibited severely distorted shape. Control nuclei had intensely stained heterochromatic regions and weakly stained euchromatic regions that were distributed mutually exclusively. Notably, the heterochromatic regions preferentially accumulated along with the envelope in control nuclei. In contrast, we could find neither typical heterochromatin structure nor typical euchromatin structure in HP1-depleted nuclei; HP1-depleted nuclei were uniformly stained with intermediate intensity between typical heterochromatic regions and typical

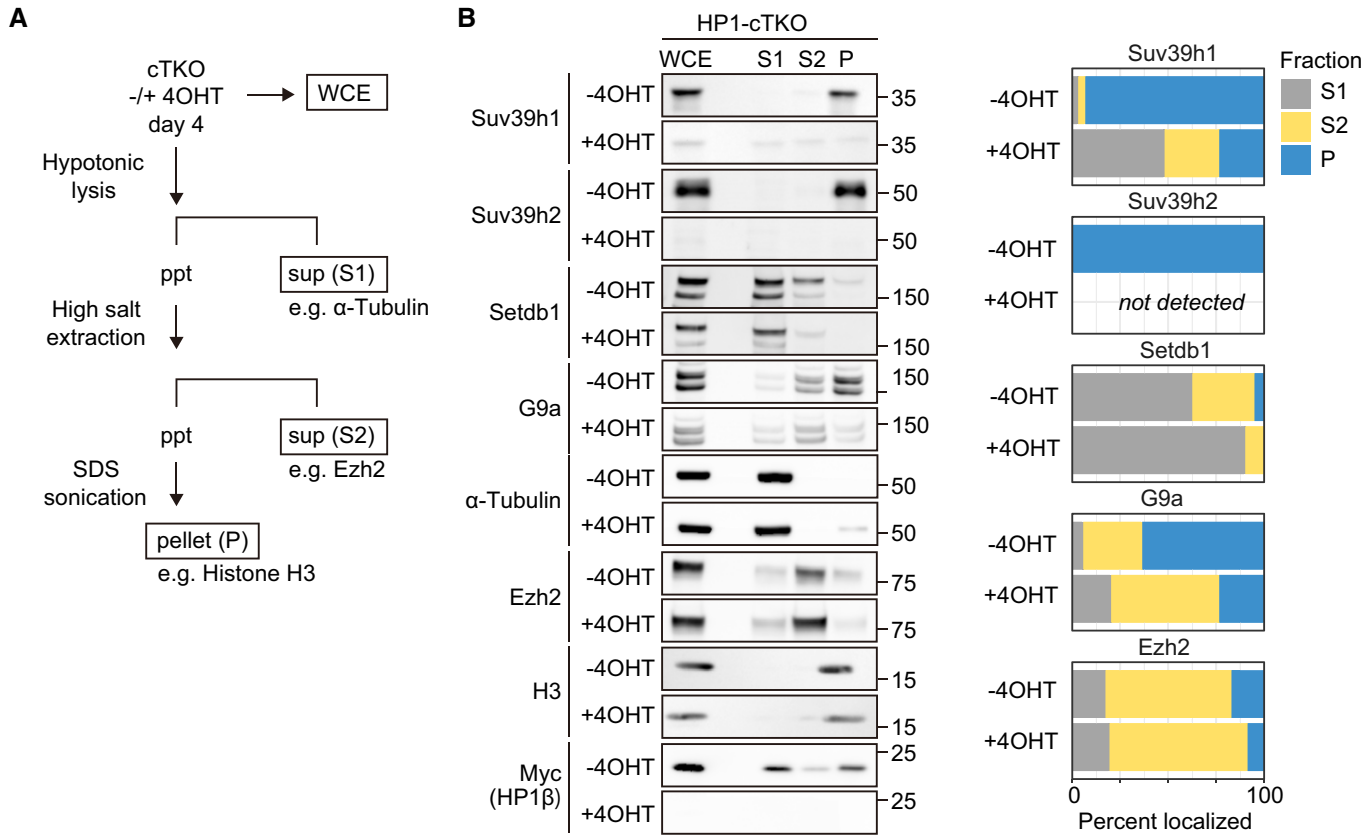

Figure 3. HP1 regulates subcellular localization of H3K9 MTs.

A Schematic illustration of the subcellular fractionation of mESCs. Fractions S1, S2, and P are mainly composed of cytosolic proteins, nuclear soluble proteins, and chromatin-bound proteins, respectively. The fractionating protocol is described in the materials and methods.

B Subcellular distribution of H3K9 MTs in the HP1-cTKO cells was examined by immunoblotting. α-Tubulin, Ezh2, and histone H3 were used as representative markers for each fraction. Stacked bar plots show the abundance ratios of H3K9 MTs among the three fractions (right).

Source data are available online for this figure.

euchromatic regions of control nuclei. These results indicate that HP1 plays a fundamental role in maintaining heterochromatic and euchromatic regions in mESCs.

HP1 regulates subcellular localization of H3K9 MTs

To further address the mode of action of HP1-mediated protein integrity regulation of H3K9 MTs, we examined subcellular localization of H3K9 MTs in the presence and absence of HP1. We prepared three subcellular fractions from mESC lysates and examined their protein compositions (Fig 3A and B). Fractions S1, S2, and P mainly comprise cytosolic proteins, nuclear soluble proteins, and chromatin-bound insoluble proteins, respectively (Kappes *et al*, 2001). We found that most Suv39h1/2 proteins (> 90%) were detected in fraction P in the presence of HP1. However, in the absence of HP1, the proportion of chromatin-bound Suv39h1 was drastically reduced (~25%). These results indicate that Suv39h1 was released from chromatin by HP1 depletion. A previous study showed that Setdb1 is a cytoplasmic/nuclear shuttling protein (Timms *et al*, 2016). We found that ~40% of Setdb1 was localized in the nucleus (fractions S2+P) in the presence of HP1, whereas the proportion of nuclear localized Setdb1 was reduced to less than 10% by HP1 depletion, indicating that HP1 ensures nuclear localization of Setdb1. Dominant proportion of G9a (> 60%) was detected in fraction P in the presence of HP1. However, HP1 depletion led to a drastic reduction in this proportion (~25%), indicating that HP1 anchors G9a to chromatin. In contrast to H3K9 MTs, subcellular localization of H3K27MT Ezh2 remained almost unchanged by HP1 depletion. Taking these results together, we concluded that HP1 specifically confines H3K9 MTs to chromatin.

HP1 ensures protein stability of H3K9 MTs by confining them to chromatin

We then dissected the molecular functions of the chromodomain and chromoshadow domain of HP1 in protein stability regulation of H3K9 MTs. We generated expression constructs of HP1β mutants (Fig 4A), one of which harbored a V23M substitution in the chromodomain that abolishes the binding affinity to H3K9 methylation (Bannister *et al*, 2001), and the other harbored an I161E substitution in the chromoshadow domain that abolishes dimerization (Brasher *et al*, 2000). Co-immunoprecipitation followed by immunoblotting indicated that HP1β (V23M) formed dimers and interact with Suv39h1 and Setdb1, but could not bind to H3K9me3 (Fig 4B). We found that HP1β (I161E) lost all of these abilities (Fig 4B and summarized in Fig 4A). Previous studies demonstrated that automethylated G9a at ARKT motif binds to chromodomain of HP1 (Chin *et al*, 2007; Sampath *et al*, 2007). However, we found that HP1β (V23M) still binds to G9a/GLP complex (Fig 4C). We therefore propose that G9a/GLP complex binds to HP1 both in an automethylation-dependent manner and an automethylation-independent manner. Accordingly, a previous study demonstrated that HP1 dimerization is required for its binding to G9a/GLP complex (Nozawa *et al*, 2010). Similarly, we also found that dimerization-defective HP1β (I161E) lost its binding ability to G9a/GLP complex (Fig 4C).

We next established a series of HP1-cTKO lines expressing essentially equal amounts of wild type, V23M, or I161E of Flag-HP1β (Fig 4D), and then incubated them with 4OHT to excise the previously introduced *Myc-hHP1β* transgene. The protein levels of Suv39h1/2, Setdb1, and G9a/GLP complex were maintained in the HP1-cTKO line expressing wild-type Flag-HP1β even after 4OHT treatment, whereas those were decayed in the HP1-cTKO lines expressing Flag-HP1β mutants (Fig 4E). Thus, we concluded that not only HP1-H3K9 MT interaction but also HP1-H3K9me2/3 interaction is crucial for maintaining protein stability of H3K9 MTs.

Cell viability analysis demonstrated that the HP1-cTKO line expressing wild-type Flag-HP1β was viable even after 4OHT treatment, whereas those expressing Flag-HP1β (V23M) or (I161E) were not (Fig EV4A), indicating that HP1-H3K9me2/3 interaction is crucial for ensuring cellular viability. As shown in Fig EV4B, the proportion of chromatin-bound H3K9 MTs was almost unchanged in the HP1-cTKO line carrying an additional transgene of wild-type *Flag-HP1β* after 4OHT treatment. In contrast, those proportions were drastically reduced in the HP1-cTKO line carrying an additional transgene of *Flag-HP1β* mutants after 4OHT treatment. These results indicate that H3K9me2/3-HP1 interaction and HP1 dimerization are crucial for ensuring protein stability of H3K9 MTs.

HP1 stabilizes H3K9 DMs, Jmjd1a and Jmjd1b, at the protein level

Jmjd1a is an H3K9 DM that catalyzes H3K9me2 demethylation (Yamane *et al*, 2006). We previously demonstrated that the H3K9me2 levels are correctly tuned through methylation by G9a/GLP complex and demethylation by Jmjd1a and its related paralog, Jmjd1b (Kuroki *et al*, 2018). If HP1 plays a fundamental role in the tuning of H3K9me2, HP1 might also be involved in the protein stability regulation of Jmjd1a/b. To validate this hypothesis, we first examined protein–protein interaction between HP1 and Jmjd1a/b (Fig 5A). Intriguingly, co-immunoprecipitation followed by immunoblotting indicated that endogenous HP1β interacts with endogenous Jmjd1a and Jmjd1b. We then performed protein decay analysis using HP1-cTKO cells (Fig 5B). Immunoblot showed that Jmjd1a/b protein decayed in HP1-cTKO cells after 4OHT treatment concomitantly with the decrease of Myc-HP1β. Quantified protein levels of Jmjd1a and Jmjd1b were, respectively, reduced to 8% and 5% in HP1-cTKO cells 4 days after 4OHT treatment. RT-qPCR indicated that the mRNA levels of *Jmjd1a* and *Jmjd1b* were essentially unchanged by HP1 depletion (Fig EV5A), indicating that HP1 stabilizes Jmjd1a/b at the protein level. Protein stability analysis using cTKO cells carrying an additional transgene of Flag-tagged HP1 confirmed that all HP1 paralogs exhibit the ability to ensure protein stability of Jmjd1a/b (Fig EV5B). The proportion of chromatin-bound Jmjd1a/b was also reduced in HP1-cTKO cells after 4OHT treatment (Fig EV5C).

We next elucidated whether HP1β (V23M) and (I161E) could maintain the protein levels of Jmjd1a/b. As shown in Fig 5C, wild-type HP1β rescued the protein decay of Jmjd1a/b, but HP1β (V23M) and (I161E) could not. This series of experiments indicates that HP1 ensures protein stability of Jmjd1a/b by tethering these enzymes to chromatin.

H3K9me2/3 is required for maintaining protein stability of Jmjd1a/b

We hypothesized that Jmjd1a/b might be destabilized in mESCs that completely lack H3K9me2/3, as it was expected that HP1 could no

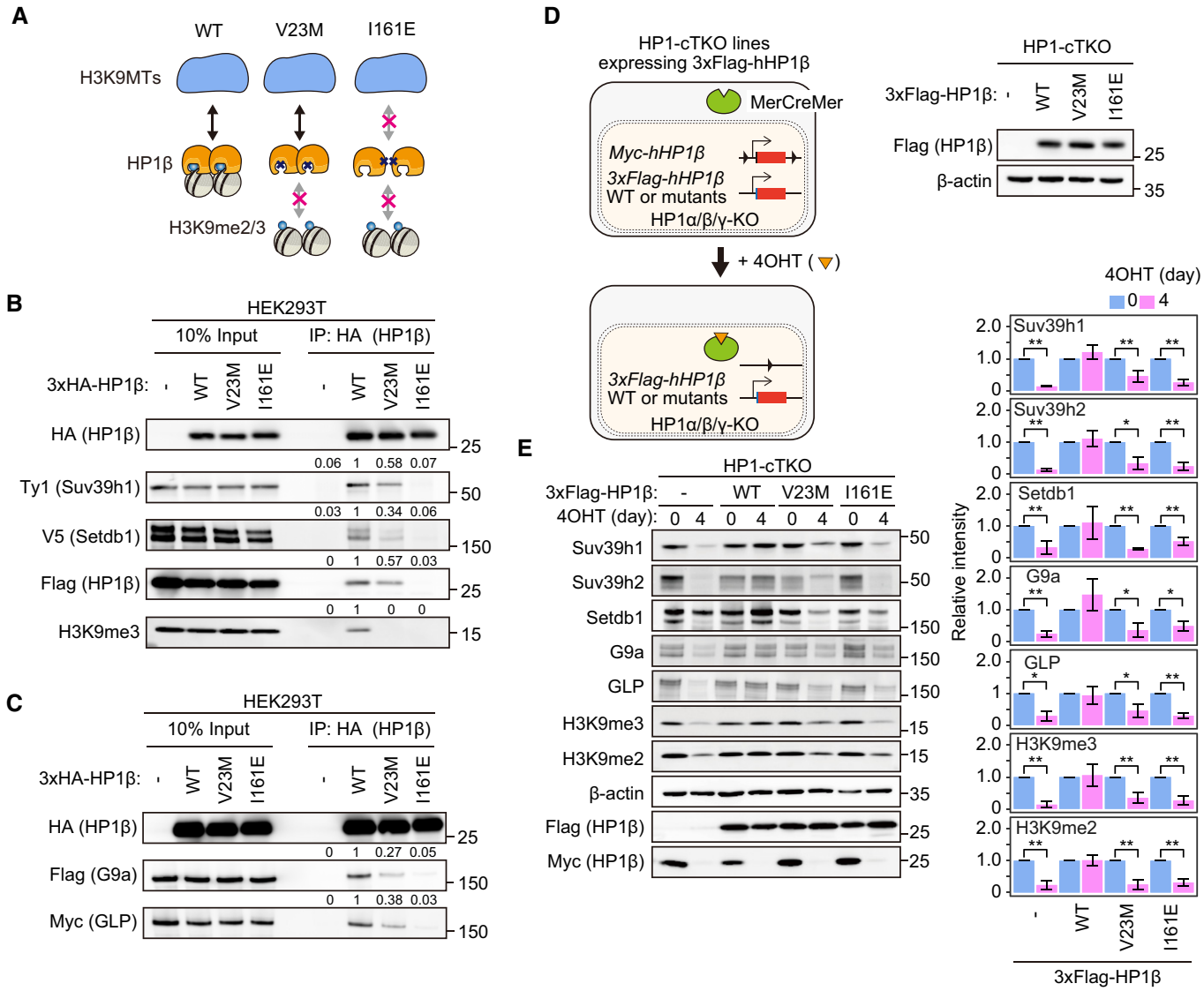

Figure 4. HP1 ensures protein stability of H3K9 MTs by confining them to chromatin.

A Schematic illustration of HP1 mutants used in this study. V23M and I161E mutants lose the ability to bind H3K9me3 and to form dimers, respectively.

B, C Elucidation of protein–protein interaction between HP1 and H3K9 MTs by co-immunoprecipitation analysis. Whole-cell extracts of HEK293T cells expressing HA-HP1β mutants with epitope-tagged H3K9 MTs and HP1β were subjected to immunoprecipitation with the anti-HA tag antibody. The immunocomplex was analyzed by immunoblotting with the indicated antibodies. The intensities were quantified using ImageJ software, normalized, and shown on the top.

D Strategy to establish mESCs solely expressing mutated HP1 (left). We introduced expression constructs for 3xFlag-hHP1β (wild type or mutants) into HP1-cTKO cells and then deleted the formerly introduced wild-type *Myc-hHP1β* transgene by 4OHT treatment.

E Evaluation of HP1β mutants for maintaining H3K9me2/3 and ensuring protein stability of H3K9 MTs. H3K9me2/3 levels and the protein levels of H3K9 MTs in HP1-cTKO lines expressing 3xFlag-hHP1β mutants were compared before and after 4OHT treatment. The intensities were quantified with ImageJ software and are summarized on the right. Data represented as mean ± SD ($n > 3$, biological replicates). *$P < 0.05$, **$P < 0.01$ (Welch's test).

Source data are available online for this figure.

longer confine Jmjd1a/b to chromatin in the absence of H3K9me2/3 (Fig 6A). To evaluate this hypothesis, we established an mESC line (3S1G), in which Suv39h1/2, Setdb1, and G9a are designed to be disrupted in the presence of 4OHT (Fig 6B). Importantly, Jmjd1a/b proteins decayed massively in 3S1G cells after 4OHT treatment, in which H3K9m2/3 was virtually undetectable due to the loss of Suv39h1/2, Setdb1, and G9a (Fig 6C). On the other hand, the protein levels of Jmjd1a/b maintained in mESCs lacking Suv39h1/2 and Setdb1, in which H3K9me2 was maintained but H3K9me3 was depleted. Similarly, the protein levels of Jmjd1a/b also maintained in mESCs lacking G9a, in which H3K9me2 was depleted but H3K9me3 was maintained. These results suggest that H3K9me2/3 is crucial for the protein stability regulation of Jmjd1a/b and that either modification is sufficient for this regulation. In the model shown in Fig 6A, HP1 might be released from chromatin when H3K9me2/3 was abolished. To address this, we compared

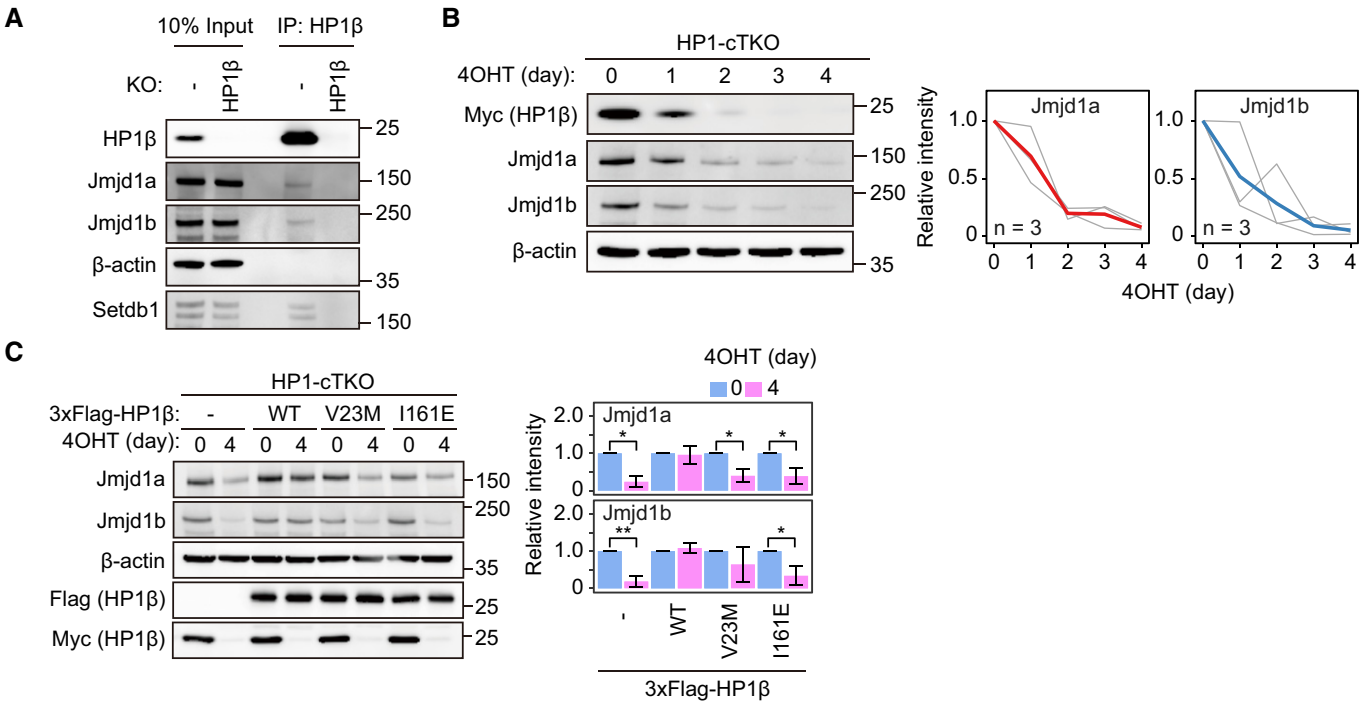

Figure 5. HP1 stabilizes H3K9 DMs, Jmjd1a and Jmjd1b, at the protein level.

A Elucidation of protein–protein interaction between HP1 and Jmjd1a/b by co-immunoprecipitation analysis. Whole-cell extracts of wild-type mESCs and HP1β-deficient mESCs were subjected to immunoprecipitation with the anti-HP1β antibody. The immunocomplex was then analyzed by immunoblotting with the indicated antibodies.

B Protein expression levels of Jmjd1a/b in HP1-cTKO cells were monitored by immunoblotting. The intensities were quantified using ImageJ software and summarized on the right. The thin gray line and bold colored line show individual data and the mean of experimental replicates, respectively.

C Evaluation of HP1β mutants for ensuring protein stability of Jmjd1a/b. The protein levels of Jmjd1a/b in HP1-cTKO lines expressing 3xFlag-hHP1β mutants were compared before and after 4OHT treatment. The intensities were quantified with ImageJ software and summarized on the right. Data represented as mean ± SD ($n > 3$, biological replicates). *$P < 0.05$, **$P < 0.01$ (Welch's test).

Source data are available online for this figure.

subcellular localization of HP1 in wild-type TT2 cells and 4OHT-treated 3S1G cells (Fig 6D). We found that HP1 proteins were detected predominantly in chromatin-bound fraction in TT2 cells. Strikingly, 4OHT treatment resulted in a dramatic reduction in the proportion of chromatin-bound HP1. These results further support the importance of HP1-mediated tethering of Jmjd1a/b to chromatin for ensuring protein stability of Jmjd1a/b.

Finally, we examined cell viability of mESCs lacking H3K9 MTs. mESCs lacking Suv39h1/2, Setdb1, and G9a exhibited severe growth defects similar to those lacking HP1α/β/γ (Fig EV5D), indicating the importance of the H3K9 MTs-HP1-H3K9me2/3 axis for mESC viability.

Discussion

Our findings indicate that mammalian HP1 is not just a simple reader of H3K9me2/3 but forms an essential hub for heterochromatin organization. A previous study showed that artificial tethering of HP1 on transcriptionally active chromatin could generate ectopic

Figure 6. H3K9me2/3 is required for maintaining protein stability of Jmjd1a/b.

A A model of HP1-mediated protein stability regulation of Jmjd1a/b. In wild-type cells, HP1 tethers Jmjd1a/b to chromatin through HP1-H3K9me2/3 interaction. We speculated that HP1 might be released from chromatin in Suv39h/Setdb1/G9a-deficient cells since H3K9me2/3 might be absent in these cells. In this situation, HP1 might no longer ensure protein stability of Jmjd1a/b.

B Strategy to establish Suv39h/Setdb1/G9a-deficient mESCs. By disrupting *G9a* alleles in the #33-6-SuvDKO line by CRISPR/Cas, we established an mESC line, 3S1G, which carries the conditional knockout alleles for *Setdb1* and conventionally knocked out alleles for *Suv39h* and *G9a*.

C Impact of Suv39h/Setdb1/G9a depletion on HP1-mediated protein stability regulation of Jmjd1a/b. Jmjd1a/b was destabilized in mESCs lacking Suv39h/Setdb1/G9a, even though HP1 was present.

D Functional evaluation of H3K9me2/3 for confining HP1 to chromatin. Subcellular localizations of HP1α, β, and γ in TT2 and mESCs lacking Suv39h/Setdb1/G9a were compared. α-Tubulin, Ezh2, and histone H3 were used as representative markers for each fraction.

Source data are available online for this figure.

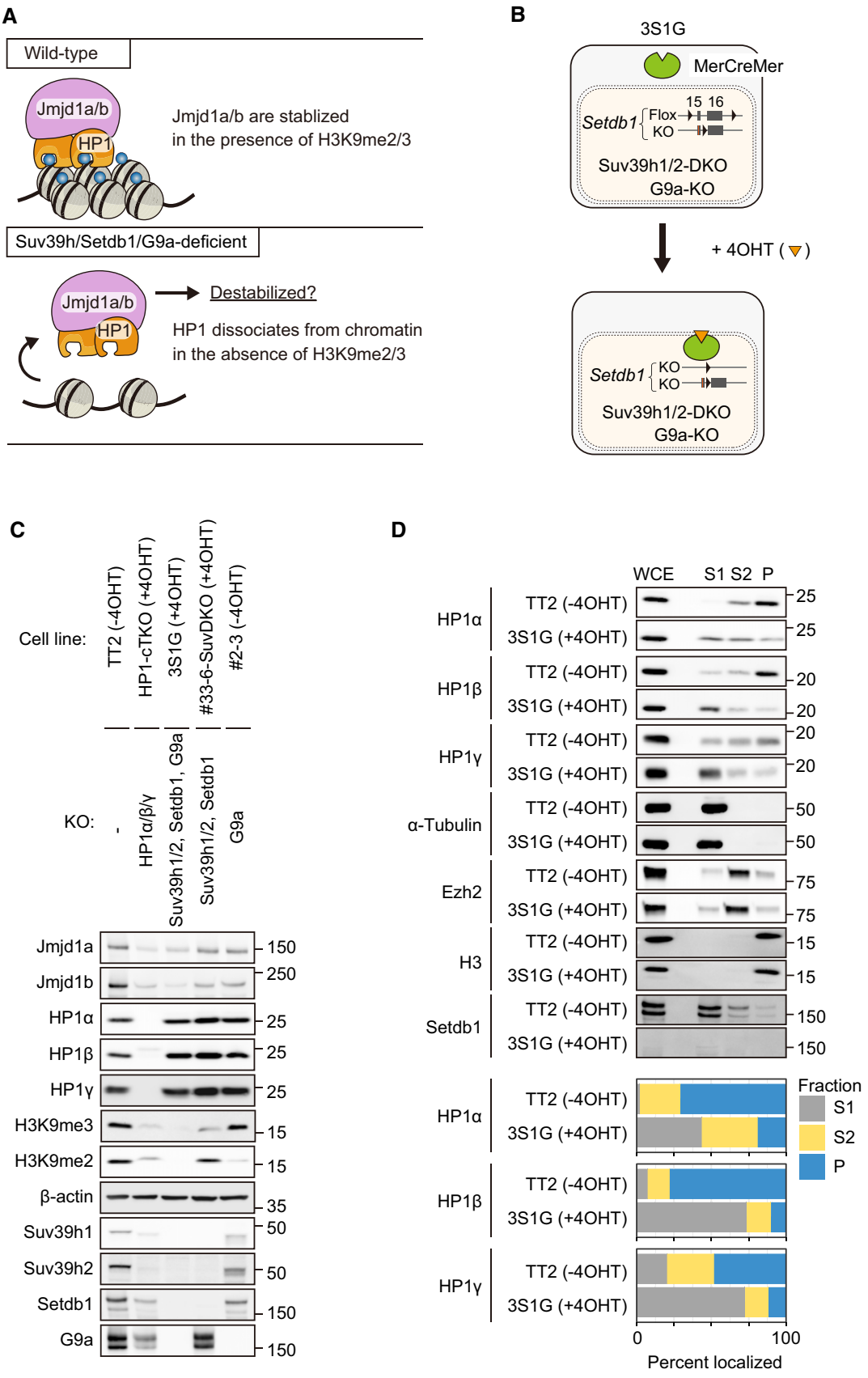

Figure 6.

heterochromatin (Hathaway *et al*, 2012), which supports our results. Fission yeast contains an HP1 ortholog Swi6 and a Suv39h1 ortholog Clr4, serving as a good model for understanding heterochromatin organization (Jih *et al*, 2017). However, in contrast to mammals, Swi6 depletion does not reduce H3K9me3 in fission yeast (Jih *et al*, 2017). This fact indicates that H3K9 methylation by Clr4 is achieved independently of Swi6. Accordingly, artificial tethering of Swi6 on transcriptionally active chromatin could not generate ectopic heterochromatin in fission yeast (Rani *et al*, 2019). We therefore speculate that the function of HP1 as the master organizer of heterochromatin might have evolved in higher eukaryotes.

Intriguingly, in contrast to H3K9me2/3 levels, H3K9me1 level was maintained in mESCs lacking HP1. A previous study demonstrated that H3K9me1 is produced in the cytoplasm by Prdm3 and Prdm16 (Pinheiro *et al*, 2012). As HP1 localizes in nucleus, it is plausible that HP1 depletion might not affect H3K9me1-producing pathway in cytoplasm.

Our present study indicates that HP1 paralogs act redundantly in terms of maintaining heterochromatin and ensuring cell viability in mESCs. On the other hand, genetic studies have suggested paralog-specific functions of HP1. HP1β-deficient mice exhibit distorted neurogenesis and die around the neonatal period (Aucott *et al*, 2008). Germ cell development is dysregulated in HP1γ-deficient mice; the proliferation of primordial germ cells lacking HP1γ is defective (Abe *et al*, 2011), and HP1γ-deficient male germlines cannot complete meiosis (Takada *et al*, 2011). It has been shown that the post-transcriptional modification of HP1 occurs in a paralog-specific manner. For example, phosphorylation of the N terminus of HP1α strengthens affinity for H3K9me3-modified nucleosomes and plays a vital role in phase separation (Hiragami-Hamada *et al*, 2011; Larson *et al*, 2017; Strom *et al*, 2017). Phosphorylation of the HP1γ chromoshadow domain might play a role in the DNA damage repair response (Akaike *et al*, 2015). It is plausible that these paralog-specific modifications of HP1 might be crucial in cells other than mESCs. Unlike mESCs, previous study has shown that mouse embryonic liver cell lines lacking all HP1 paralogous are viable (Saksouk *et al*, 2020), suggesting the distinct role of HP1 in ensuring cell viability between cell types.

The most important finding in our study is that HP1 comprehensively regulates protein stability of enzymes involved in H3K9me2/3 dynamics. The next important step for understanding the biological significance of this finding is to uncover the protein degradation machinery of these enzymes. Because Mdm2 and Dcaf13 are implicated in the ubiquitin–proteasome-dependent degradation of Suv39h1 (Bosch-Presegué *et al*, 2011; Zhang *et al*, 2018), multiple E3 ubiquitin ligases might be involved in Suv39h1 protein degradation. A previous study demonstrated, APC/C^{Cdh1} is involved in the degradation of G9a/GLP in senescent cells (Takahashi *et al*, 2012); thus, it may be worth investigating the relationship between HP1 and cellular senescence. To date, very little is known about the molecular mechanisms of protein degradation of H3K9 DMs. Many studies have shown that H3K9me2/3 is dynamically re-organized during mammalian development (Rao *et al,* 2017; Nicetto & Zaret, 2019). Furthermore, aberrant H3K9me2/3 levels were frequently observed in cancer (Saha & Muntean, 2021) and neural diseases (Ryu *et al*, 2006; Chase *et al*, 2013). Thus, we propose that the molecular machinery facilitating protein degradation of H3K9 MTs and/or H3K9 DMs possibly contributes to the dynamic organization of heterochromatin during mammalian development and disease onset.

Materials and Methods

Cell culture

mESCs were maintained in Dulbecco's Modified Eagle's Medium (Nacalai Tesque, Japan) containing 10% knockout SR (Invitrogen, USA), 1% fetal calf serum, 1% sodium pyruvate (Gibco, Carlsbad, CA, USA), 1% Minimum Essential Medium Non-Essential Amino Acids (Gibco), and 10^3 U/ml of leukemia-inhibiting factor. We maintained 293T cells in Dulbecco's Modified Eagle's Medium containing 10% fetal calf serum, 1% sodium pyruvate (Gibco), and 1% Minimum Essential Medium Non-Essential Amino Acids (Gibco). For conditional knockout of HP1 or Setdb1, mESCs were cultured in the presence of 800 nM 4OHT. To investigate protein stability of Suv39h1 and Setdb1, the cells were treated with 50 μg/ml cycloheximide alone or in combination with 5 μM MG132.

Plasmids

For construction of mammalian expression vectors, cDNA of HP1α/-β/γ, Suv39h1, Setdb1, G9a, GLP, and ubiquitin was inserted into pCAG-IRES-blasticidin or puromycin vector with epitope tag sequence by DNA assembly technology using NEBuilder HiFi DNA Assembly Master Mix (New England BioLabs, USA). For construction of knockout vectors, gRNA sequence of these genes was inserted into pX330 vector. For construction of bacterial expression vectors, cDNAs of HP1β and Setdb1 (575-1308) were inserted into pET28a and pGEX4T2 vector, respectively.

Immunoblotting

Cell lysates were dissolved in 1x sodium dodecyl sulfate (SDS) sample buffer (62.5 mM Tris-HCl, 2% SDS, 5% sucrose, 5% 2-mercaptoethanol, and bromophenol blue), sonicated, and boiled for 5 min. The lysate was resolved by SDS polyacrylamide gel electrophoresis and transferred to nitrocellulose membranes. Nonspecific protein binding was blocked with 5% skim milk/TBST (10 mM Tris-HCl, 150 mM NaCl, 0.1% Tween-20) for 30 min at 27°C, then the membranes were probed with primary antibodies in Signal enhancer HIKARI (Nacalai) at 4°C overnight. The membranes were then incubated with HRP-conjugated antibodies against mouse, rabbit, and rat IgG in 5% skim milk/TBST at 4°C for 2 h, then visualized using enhanced chemiluminescence kits (PerkinElmer Life and Analytical Sciences, USA).

Generation of HP1-deficient mESCs

To establish HP1 double-knockout mESC lines, pX330 plasmids containing gRNA of HP1β or HP1γ and 50 ng pCAG-puro (which confers puromycin resistance) were introduced into mESCs using Lipofectamine 2000 (Invitrogen). Twenty-four hours after transfection, the cells were re-plated and cultured in the presence of 1 μg/μl puromycin for 24 h. After treatment for ~2 weeks, candidate colonies were isolated and identified by genomic sequencing and immunoblotting. HP1β/α-deficient cells were generated by introduction into

HP1β-deficient cells with the pX330 plasmid containing gRNA of HP1α. HP1γ/α-deficient cells and HP1γ/β-deficient cells were generated by introduction into HP1γ-deficient cells with pX330 plasmid containing gRNA of HP1α and HP1β, respectively. To establish HP1 triple-knockout mESC line, loxP-pCAG-Myc-HP1β-loxP vector and pCAG-hygromycin were introduced into HP1γ/β-deficient cells. After 100 μg/μl hygromycin selection, HP1γ/β-deficient cells stably expressing Myc-HP1β were established. Cells were then transfected with the pX330 plasmid containing gRNA of HP1β to disrupt endogenous HP1β alleles. After isolation of endogenous HP1α/β/γ-deficient cells (containing loxP-Myc-HP1β-loxP sequence), cells expressing merCremer were established by introduction with pCAG-merCremer-IRES-zeocin vector and 100 μg/μl zeocin selection.

Generation of H3K9 MTs-deficient mESCs

Setdb1 conditional knockout mESCs were generated in a previous study (Matsui *et al*, 2010). We established Setdb1, Suv39h1, and Suv39h2 triple-knockout mESC line (#33-6-SuvDKO), by transfecting Setdb1 conditional knockout mESCs with pCAG-puro pX330 plasmids containing gRNA of Suv39h1 and Suv39h2. After 1 μg/μl puromycin selection for 24 h and subsequent treatment, candidate colonies were isolated and identified by genomic sequencing and immunoblotting. Suv39h/Setdb1/G9a-KO cells were generated by introduction into #33-6-SuvDKO with triple multiplex pX330 plasmids containing gRNA of G9a. After 1 μg/μl puromycin selection for 24 h and subsequent treatment, candidate colonies were isolated and identified by immunoblotting. Mutated alleles for Suv39h1 and Suv39h2 in H3K9 MTs-deficient mESCs are summarized in Table 2.

Immunofluorescence

Cells were fixed with 4% paraformaldehyde in PBS (pH 7.4) for 10 min. After permeabilization and blocking nonspecific protein binding with IF buffer (PBS, 0.5% Triton X-100, 2% skim milk) for 30 min, cells were incubated with primary antibodies in IF buffer at 4°C overnight. Cells were then incubated with Alexa Flour-conjugated antibodies against mouse, rabbit, and rat IgG and DAPI in IF buffer at 4°C for 2 h. Cells were then observed with a confocal laser scanning microscope (LSM700, Carl Zeiss, Germany) and imaged using ZEN software on an LSM700 microscope. ImageJ was used to process the images, and quantitative intensity values were visualized using R software (ver. 3. 5. 1).

Transmission electron microscopy

Cells were prefixed overnight with 2.5% glutaraldehyde in 0.15 M phosphate buffer (pH 7.4). After removing the supernatant, the pellet was embedded in 2% agarose and cut into pieces. The samples were then post-fixed with 1% osmium tetroxide for 6 h, dehydrated in a graded ethanol series, and embedded in epoxy resin (Nisshin EM, Japan). Ultrathin sections were cut using a diamond knife on an ultramicrotome (Leica EM UC7, Leica, Austria). The sections were stained with uranyl acetate for 20 min and lead acetate for 5 min. The specimens were observed under a Hitachi H-7500 electron microscope at an accelerating voltage of 80 kV.

Preparation of recombinant protein

Preparation of recombinant protein was performed as described previously (Rea *et al*, 2000). Briefly, the bacterial expression vectors were introduced into *E. coli* strain BL21. The expression of recombinant proteins was induced by 0.4 mM isopropyl 1-thio-b-D-galactopyranoside. The recombinant proteins were solubilized in RIPA buffer (20 mM Tris pH 7.5, 500 mM NaCl, 5 mM EDTA, 1% NP-40, 0.5% sodium deoxycholate, and protease inhibitor (PI) mixture (Roche, Switzerland)) by sonication. GST-tagged and His-tagged proteins were purified using Glutathione Magnetic Agarose

Table 2. Mutated alleles for H3K9 MTs-KO mESCs.

Line	Target	Allele	Sequence	Mutation
Suv39h/Setdb1-KO clone #33-6-SuvDKO	*Suv39h1*	WT allele	CTGCAGGACCTGTGCCGACTAGCCAAGCTTTCT	–
		KO allele	CTGCAGGACCTGTGCC--------AAGCTTTCT	−8 bp
	Suv39h2	WT allele	CTACTACATTAACGAGTACAGGCCAGCTCCCGG	–
		KO allele1	CTA----------AAGCTCCCGG	−21 + 1 bp
		KO allele2	CTA----------AAGCTCCCGG	−21 + 1 bp
Suv39h/Setdb1 /G9a-KO clone 3S1G	*Suv39h1*	WT allele	CTGCAGGACCTGTGCCGACTAGCCAAGCTTTCT	–
		KO allele	CTGCAGGACCTGTGCC--------AAGCTTTCT	−8 bp
	Suv39h2	WT allele	CTACTACATTAACGAGTACAGGCCAGCTCCCGG	–
		KO allele1	CTA----------AAGCTCCCGG	−21 + 1 bp
		KO allele2	CTA----------AAGCTCCCGG	−21 + 1 bp
	G9a	WT allele	GAGGGGCAGCCCAAAGTGCACCGAGCCCGGAAA	–
		KO allele	Not determined	
	G9a	WT allele	AGATGTGGCCAAAAGGAGGAAGCTGAACTCTGG	–
		KO allele	Not determined	
	G9a	WT allele	AGGAGAGCTGATCTCTGATGCCGAGGCTGATGT	–
		KO allele	Not determined	

Underlines in WT alleles represent the PAM sequence.

Beads (Thermo Fisher Scientific, USA) and TALON Magnetic Beads (Takara Bio, Japan), respectively.

Immunoprecipitation

We suspended cells in micrococcal nuclease (MNase) buffer (20 mM Tris-HCl pH 8.0, 5 mM NaCl, 2.5 mM $CaCl_2$, 1 mM $MgCl_2$, and PI mixture) and digested the cells with MNase (Takara Bio) at 37°C for 10 min to extract nucleosome-bound proteins. After adding 4× volume of IP buffer (50 mM Tris-HCl pH 8.0, 150 mM NaCl, 10 mM EDTA, 10% glycerol, 0.1% Nonidet P-40, and PI mixture), the cell extracts were sonicated. Supernatants obtained by centrifugation were incubated with complexes comprising anti-Flag or HA antibody and Dynabeads Protein G (VERITAS, Japan) at 4°C for 2 h. The precipitates were boiled for 5 min in SDS sample buffer. The denatured protein extract was analyzed by immunoblotting.

In vitro pull-down assay

Bacteria cells and 293T cells expressing Setdb1 (575-1308) were lysed with RIPA buffer, followed by sonication. The extracts were incubated with complexes comprising His-HP1β and TALON Magnetic beads at 4°C for 2.5 h. The precipitates were boiled for 5 min in SDS sample buffer. The denatured protein extract was analyzed by immunoblotting.

HMT activity assay

HMT activity assay was performed as described previously (Tachibana *et al*, 2001). Briefly, 3xFlag-Setdb1 purified from HEK293T were mixed with recombinant GST-fused N-terminal tail of histone H3, 160 μM S-adenosylmethionine in HMT buffer (50 mM Tris-HCl pH8.8, 5 mM $MgCl_2$, and 4 mM DTT). The mixtures were incubated at 25°C for 60 min. The reaction products were boiled for 5 min in SDS sample buffer and subjected to immunoblotting.

RT-qPCR

Total RNA was extracted using the AllPrep DNA/RNA Mini Kit (Qiagen, Netherlands). cDNA was synthesized using ReverTra Ace qRT-PCR RT Master Mix (Toyobo, Japan) and amplified using TB Green Premix Ex Taq II Tli RNase H plus (Takara). The primers used are listed in Table 3.

Subcellular fractionation

Subcellular fractionation was performed as described previously (Kappes *et al*, 2001) with some modifications. First, cells (without freezing) were suspended in hypotonic buffer S1 (10 mM Hepes-KOH pH 7.9, 10 mM KCl, 0.34 M sucrose, 1.5 mM $MgCl_2$, 0.5% NP-40, and PI mixture) and incubated on ice for 10 min. After centrifugation at 1,000 *g* for 5 min, the supernatant was collected. This process was repeated once again, and the supernatant was collected as fraction S1. The pellet was then suspended in high-salt buffer S2 (10 mM Hepes-KOH pH 7.9, 450 mM NaCl, 0.34 M sucrose, 3 mM EDTA, 0.2 mM EGTA, and PI mixture) and incubated at 4°C for 20 min with vortexing. After centrifugation at 12,000 *g* for 5 min, the supernatant was collected. This process was repeated once again; the supernatant was collected as the fraction S2. The pellet was dissolved in SDS sample buffer containing 450 mM NaCl and shared by sonication, and the fraction was collected as fraction P.

Table 3. RT-qPCR primers.

Primer	Sequence (5′→3′)
Suv39h1_RT_1F	AATCGACTGCGCGTCCC
Suv39h1_RT_1R	TCCGCCATCTTTCTCCACAG
Suv39h1_RT_2F	TAGAAGCTGGGGTTGAGTTGC
Suv39h1_RT_2R	TAAGGGGCCCCAAATAGGAA
Suv39h1_RT_3F	GTTCTCTCTGTACCCCTCAGC
Suv39h1_RT_3R	ACTCAACCCCAGCTTCTAACC
Suv39h2_RT_1F	CAGACTCCATTGACCACAGCC
Suv39h2_RT_1R	AGCTCCGTTTCCTGACACTTC
Suv39h2_RT_2F	AACCCAATGTAAATGTGGAGCC
Suv39h2_RT_2R	TGAGCTCCGTTTCCTGACACT
Suv39h2_RT_3F	GAGTGGGTAGGCCTTTGGAC
Suv39h2_RT_3R	GGCAGAGCTGAGGAGTTCAC
Setdb1_RT_1F	CGCTGCAATTGTGACCCAAA
Setdb1_RT_1R	ACAGCTGTAGTCGAACCTGC
Setdb1_RT_2F	CAACCAACATGGCTTCCGTG
Setdb1_RT_2R	GGCCTAGGTTGCCTTCAAGT
Setdb1_RT_3F	AGTTTAAGCCCATGGAGCCC
Setdb1_RT_3R	CGTGATTGTGCAAGTTGGCT
G9a_RT_1F	CATCCCTGTCCGGGTTTTCA
G9a_RT_1R	TCGGTCACCGTAGTCAAAGC
G9a_RT_2F	CAAGATTGACCGCATCAGCG
G9a_RT_2R	GGTCTCCCGCTTAAGGATGG
G9a_RT_3F	GATCTACGGTTCCCACGCAT
G9a_RT_3R	GTCACCGTAGTCAAAGCCCA
GLP_RT_1F	AGTCTCAGTTCGCAGGTGTG
GLP_RT_1R	CGATATCCCTGCTCACCGTC
GLP_RT_2F	CAGGATGACGGTGGATGGAC
GLP_RT_2R	TAGACAGCAGCAGCTTCACC
GLP_RT_3F	TGACTGCTCCTCTAGCACCT
GLP_RT_3R	GATCAAGGGTGGTTCTGCCA
Jmjd1a_RT_1F	GGAAGAACTGCCAACAGGGT
Jmjd1a_RT_1R	TGTGTGGGCATCAGGTTCTC
Jmjd1a_RT_2F	TGGGAATGTCAACAAGGAGA
Jmjd1a_RT_2R	CAGGTGTCAAGATGGTGCTG
Jmjd1a_RT_3F	GAGCCACAGTCGGAGACTTC
Jmjd1a_RT_3R	CGGCCAGTCCTTAAGTTTCA
Jmjd1b_RT_1F	GGTGCCCCAGGACCTAGCG
Jmjd1b_RT_1R	AAGTGAGCCTTCCAGCAGAA
Jmjd1b_RT_2F	AAACAGAAAGGCAGCTGGTCGC
Jmjd1b_RT_2R	CAAATCCAGAAGAGGCCAGACTA
Jmjd1b_RT_3F	CCCCTGTTTTCTCTTCATCCT
Jmjd1b_RT_3R	TTCTACCACTGAGGCGATGAT

After 3 M NaCl was added to the S1 fraction samples to adjust the concentration of NaCl, 4xSDS sample buffer was added to the S1 and S2 fraction samples, and all fraction samples were boiled for 5 min and analyzed by immunoblotting.

Antibodies

We used the following antibodies: rabbit anti-HP1α (BMP001; MBL, Japan), rabbit anti-HP1β (BMP002; MBL), mouse anti-HP1γ (MA3-054; Thermo Fisher Scientific), rabbit anti-Suv39h1 (#8729; Cell Signaling Technologies (CST), USA), rabbit anti-Suv39h2 (LS-C116360; LSBio, USA), rabbit anti-Setdb1 (11231-1-AP; Proteintech, USA), rabbit anti-Ezh2 (#5246; CST), mouse anti-H3K9me1 (CMA306 (Kimura *et al*, 2008)), mouse anti-H3K9me2 (CMA317 (Hayashi-Takanaka *et al*, 2011)), mouse anti-H3K9me3 (CMA318 (Hayashi-Takanaka *et al*, 2011)), mouse anti-H3K9ac (CMA305 (Kimura *et al*, 2008)), rabbit anti-H3K27me3 (07-449; Millipore, USA), rat anti-H3 (clone 1G1 (Maehara *et al*, 2015)), rat anti-H3 (CE-039A; CosmoBio, Japan), mouse anti-Myc (#2276; CST), mouse anti-Flag (F3165; Sigma-Aldrich, USA), rat anti-HA (11867423001; Sigma-Aldrich), mouse anti-Ty1 (C15200054; Diagenode, USA), mouse anti-V5 (R960-25; Thermo Fisher Scientific), mouse anti β-actin (A1978; Sigma-Aldrich), and rat-anti α-Tubulin (ab6160; Abcam, USA).

Statistical analysis

Data were analyzed by Welch's *t*-test and Tukey's honestly significant difference test using R software.

Data availability

This study does not include any data deposited in external repositories.

Expanded View for this article is available online.

Acknowledgements
We thank Yuko Yokota for technical assistance in generating HP1-deficient cells and Hiroshi Kimura for providing antibodies against modified histones. We thank Kaoru Mitsuoka and Kenzo Uehira for providing technical assistance with transmission electron microscopy. We also thank all members of the Tachibana laboratory. This work was supported by JSPS KAKENHI grant numbers 18H02419 (MT), 17H06424 (MT), 18K14675 (RM), and 18J00586 (RM).

Author contributions
Ryo Maeda: Conceptualization; Data curation; Formal analysis; Validation; Investigation; Visualization; Writing—original draft. **Makoto Tachibana:** Conceptualization; Supervision; Investigation; Writing—original draft; Project administration.

In addition to the CRediT author contributions listed above, the contributions in detail are:
RM and MT designed and performed the experiments. RM visualized the data. RM and MT wrote the manuscript.

Declaration and competing interests statement
The authors declare that they have no conflict of interest.

References

Aagaard L, Laible G, Selenko P, Schmid M, Dorn R, Schotta G, Kuhfittig S, Wolf A, Lebersorger A, Singh PB *et al* (1999) Functional mammalian homologues of the *Drosophila* PEV-modifier Su(var)3–9 encode centromere-associated proteins which complex with the heterochromatin component M31. *EMBO J* 18: 1923 – 1938

Abe K, Naruse C, Kato T, Nishiuchi T, Saitou M, Asano M (2011) Loss of heterochromatin protein 1 gamma reduces the number of primordial germ cells via impaired cell cycle progression in mice. *Biol Reprod* 85: 1013 – 1024

Akaike Y, Kuwano Y, Nishida K, Kurokawa K, Kajita K, Kano S, Masuda K, Rokutan K (2015) Homeodomain-interacting protein kinase 2 regulates DNA damage response through interacting with heterochromatin protein 1γ. *Oncogene* 34: 3463 – 3473

Aucott R, Bullwinkel J, Yu Y, Shi W, Billur M, Brown JP, Menzel U, Kioussis D, Wang G, Reisert I *et al* (2008) HP1-β is required for development of the cerebral neocortex and neuromuscular junctions. *J Cell Biol* 183: 597 – 606

Bannister AJ, Zegerman P, Partridge JF, Miska EA, Thomas JO, Allshire RC, Kouzarides T (2001) Selective recognition of methylated lysine 9 on histone H3 by the HP1 chromo domain. *Nature* 410: 120 – 124

Bosch-Presegué L, Raurell-Vila H, Marazuela-Duque A, Kane-Goldsmith N, Valle A, Oliver J, Serrano L, Vaquero A (2011) Stabilization of Suv39H1 by SirT1 is part of oxidative stress response and ensures genome protection. *Mol Cell* 42: 210 – 223

Brasher SV, Smith BO, Fogh RH, Nietlispach D, Thiru A, Nielsen PR, Broadhurst RW, Ball LJ, Murzina NV, Laue ED (2000) The structure of mouse HP1 suggests a unique mode of single peptide recognition by the shadow chromo domain dimer. *EMBO J* 19: 1587 – 1597

Canzio D, Chang EY, Shankar S, Kuchenbecker KM, Simon MD, Madhani HD, Narlikar GJ, Al-Sady B (2011) Chromodomain-mediated oligomerization of HP1 suggests a nucleosome-bridging mechanism for heterochromatin assembly. *Mol Cell* 41: 67 – 81

Chase KA, Gavin DP, Guidotti A, Sharma RP (2013) Histone methylation at H3K9: evidence for a restrictive epigenome in schizophrenia. *Schizophr Res* 149: 15 – 20

Chin HG, Estève PO, Pradhan M, Benner J, Patnaik D, Carey MF, Pradhan S (2007) Automethylation of G9a and its implication in wider substrate specificity and HP1 binding. *Nucleic Acids Res* 35: 7313 – 7323

Cowieson NP, Partridge JF, Allshire RC, McLaughlin PJ (2000) Dimerisation of a chromo shadow domain and distinctions from the chromodomain as revealed by structural analysis. *Curr Biol* 10: 517 – 525

Hathaway NA, Bell O, Hodges C, Miller EL, Neel DS, Crabtree GR (2012) Dynamics and memory of heterochromatin in living cells. *Cell* 149: 1447 – 1460

Hayashi-Takanaka Y, Yamagata K, Wakayama T, Stasevich TJ, Kainuma T, Tsurimoto T, Tachibana M, Shinkai Y, Kurumizaka H, Nozaki N *et al* (2011) Tracking epigenetic histone modifications in single cells using Fab-based live endogenous modification labeling. *Nucleic Acids Res* 39: 6475 – 6488

Hiragami-Hamada K, Shinmyozu K, Hamada D, Tatsu Y, Uegaki K, Fujiwara S, Nakayama J-i (2011) N-terminal phosphorylation of HP1 promotes its chromatin binding. *Mol Cell Biol* 31: 1186 – 1200

Ishimoto K, Kawamata N, Uchihara Y, Okubo M, Fujimoto R, Gotoh E, Kakinouchi K, Mizohata E, Hino N, Okada Y *et al* (2016) Ubiquitination of lysine 867 of the human SETDB1 protein upregulates its histone H3 lysine 9 (H3K9) methyltransferase activity. *PLoS One* 11: 1 – 19

Ivanov AV, Peng H, Yurchenko V, Yap KL, Negorev DG, Schultz DC, Psulkowski E, Fredericks WJ, White DE, Maul GG *et al* (2007) PHD domain-mediated

E3 ligase activity directs intramolecular sumoylation of an adjacent bromodomain required for gene silencing. *Mol Cell* 28: 823 – 837

Jenuwein T, Allis CD (2001) Translating the histone code. *Science* 293: 1074 – 1080

Jih G, Iglesias N, Currie MA, Bhanu NV, Paulo JA, Gygi SP, Garcia BA, Moazed D (2017) Unique roles for histone H3K9me states in RNAi and heritable silencing of transcription. *Nature* 547: 463 – 467

Kappes F, Burger K, Baack M, Fackelmayer FO, Gruss C (2001) Subcellular localization of the human proto-oncogene protein DEK. *J Biol Chem* 276: 26317 – 26323

Kimura H, Hayashi-Takanaka Y, Goto Y, Takizawa N, Nozaki N (2008) The organization of histone H3 modifications as revealed by a panel of specific monoclonal antibodies. *Cell Struct Funct* 33: 61 – 73

Kuroki S, Nakai Y, Maeda R, Okashita N, Akiyoshi M, Yamaguchi Y, Kitano S, Miyachi H, Nakato R, Ichiyanagi K *et al* (2018) Combined loss of JMJD1A and JMJD1B reveals critical roles for H3K9 demethylation in the maintenance of embryonic stem cells and early embryogenesis. *Stem Cell Rep* 10: 1340 – 1354

Lachner M, O'Carroll D, Rea S, Mechtler K, Jenuwein T (2001) Methylation of histone H3 lysine 9 creates a binding site for HP1 proteins. *Nature* 410: 116 – 120

Larson AG, Elnatan D, Keenen MM, Trnka MJ, Johnston JB, Burlingame AL, Agard DA, Redding S, Narlikar GJ (2017) Liquid droplet formation by HP1α suggests a role for phase separation in heterochromatin. *Nature* 547: 236 – 240

Maehara K, Harada A, Sato Y, Matsumoto M, Nakayama KI, Kimura H, Ohkawa Y (2015) Tissue-specific expression of histone H3 variants diversified after species separation. *Epigenetics Chromatin* 8: 1 – 17

Margueron R, Justin N, Ohno K, Sharpe ML, Son J, Drury WJ III, Voigt P, Martin SR, Taylor WR, De Marco V *et al* (2009) Role of the polycomb protein EED in the propagation of repressive histone marks. *Nature* 461: 762 – 767

Martens JHA, O'Sullivan RJ, Braunschweig U, Opravil S, Radolf M, Steinlein P, Jenuwein T (2005) The profile of repeat-associated histone lysine methylation states in the mouse epigenome. *EMBO J* 24: 800 – 812

Matsui T, Leung D, Miyashita H, Maksakova IA, Miyachi H, Kimura H, Tachibana M, Lorincz MC, Shinkai Y (2010) Proviral silencing in embryonic stem cells requires the histone methyltransferase ESET. *Nature* 464: 927 – 931

Mikkelsen TS, Ku M, Jaffe DB, Issac B, Lieberman E, Giannoukos G, Alvarez P, Brockman W, Kim T-K, Koche RP *et al* (2007) Genome-wide maps of chromatin state in pluripotent and lineage-committed cells. *Nature* 448: 553 – 560

Muramatsu D, Kimura H, Kotoshiba K, Tachibana M, Shinkai Y (2016) Pericentric H3k9me3 formation by HP1 interaction-defective histone methyltransferase suv39h1. *Cell Struct Funct* 41: 145 – 152

Nicetto D, Zaret KS (2019) Role of H3K9me3 heterochromatin in cell identity establishment and maintenance. *Curr Opin Genet Dev* 55: 1 – 10

Nozawa RS, Nagao K, Masuda HT, Iwasaki O, Hirota T, Nozaki N, Kimura H, Obuse C (2010) Human POGZ modulates dissociation of HP1α from mitotic chromosome arms through Aurora B activation. *Nat Cell Biol* 12: 719 – 727

O'Carroll D, Scherthan H, Peters AHFM, Opravil S, Haynes AR, Laible G, Rea S, Schmid M, Lebersorger A, Jerratsch M *et al* (2000) Isolation and characterization ofSuv39h2, a second histone H3 methyltransferase gene that displays testis-specific expression. *Mol Cell Biol* 20: 9423 – 9433

Pinheiro I, Margueron R, Shukeir N, Eisold M, Fritzsch C, Richter F, Mittler G, Genoud C, Goyama S, Kurokawa M *et al* (2012) Prdm3 and Prdm16 are H3K9me1 methyltransferases required for mammalian heterochromatin integrity. *Cell* 150: 948 – 960

Rani R, Yaseen AM, Malwade A, Sevilimedu A (2019) An RNA aptamer to HP1/Swi6 facilitates heterochromatin formation at an ectopic locus in *S. pombe*. *RNA Biol* 16: 742 – 753

Rao VK, Pal A, Taneja R (2017) A drive in SUVs: from development to disease. *Epigenetics* 12: 177 – 186

Raurell-Vila H, Bosch-Presegue L, Gonzalez J, Kane-Goldsmith N, Casal C, Brown JP, Marazuela-Duque A, Singh PB, Serrano L, Vaquero A (2017) An HP1 isoform-specific feedback mechanism regulates Suv39h1 activity under stress conditions. *Epigenetics* 12: 166 – 175

Rea S, Eisenhaber F, O'Carroll D, Strahl BD, Sun Z-W, Schmid M, Opravil S, Mechtler K, Ponting CP, Allis CD *et al* (2000) Regulation of chromatin structure by site-specific histone H3 methyltransferases. *Nature* 406: 593 – 599

Ryu H, Lee J, Hagerty SW, Soh BY, McAlpin SE, Cormier KA, Smith KM, Ferrante RJ (2006) ESET/SETDB1 gene expression and histone H3 (K9) trimethylation in Huntington's disease. *Proc Natl Acad Sci USA* 103: 19176 – 19181

Saha N, Muntean AG (2021) Insight into the multi-faceted role of the SUV family of H3K9 methyltransferases in carcinogenesis and cancer progression. *Biochim Biophys Acta Rev Cancer* 1875: 188498

Saksouk N, Hajdari S, Perez Y, Pratlong M, Barrachina C, Graber C, Grégoire D, Zavoriti A, Sarrazin A, Pirot N *et al* (2020) The mouse HP1 proteins are essential for preventing liver tumorigenesis. *Oncogene* 39: 2676 – 2691

Sampath SC, Marazzi I, Yap KL, Sampath SC, Krutchinsky AN, Mecklenbräuker I, Viale A, Rudensky E, Zhou M-M, Chait BT *et al* (2007) Methylation of a histone mimic within the histone methyltransferase G9a Regulates Protein Complex Assembly. *Mol Cell* 27: 596 – 608

Schultz DC, Ayyanathan K, Negorev D, Maul GG, Rauscher FJ (2002) SETDB1: a novel KAP-1-associated histone H3, lysine 9-specific methyltransferase that contributes to HP1-mediated silencing of euchromatic genes by KRAB zinc-finger proteins. *Genes Dev* 16: 919 – 932

Strom AR, Emelyanov AV, Mir M, Fyodorov DV, Darzacq X, Karpen GH (2017) Phase separation drives heterochromatin domain formation. *Nature* 547: 241 – 245

Sun L, Fang J (2016) E3-independent constitutive monoubiquitination complements histone methyltransferase activity of SETDB1. *Mol Cell* 62: 958 – 966

Tachibana M, Sugimoto K, Fukushima T, Shinkai Y (2001) SET domain-containing protein, G9a, is a novel lysine-preferring mammalian histone methyltransferase with hyperactivity and specific selectivity to lysines 9 and 27 of histone H3. *J Biol Chem* 276: 25309 – 25317

Tachibana M, Sugimoto K, Nozaki M, Ueda J, Ohta T, Ohki M, Fukuda M, Takeda N, Niida H, Kato H *et al* (2002) G9a histone methyltransferase plays a dominant role in euchromatic histone H3 lysine 9 methylation and is essential for early embryogenesis. *Genes Dev* 16: 1779 – 1791

Tachibana M, Ueda J, Fukuda M, Takeda N, Ohta T, Iwanari H, Sakihama T, Kodama T, Hamakubo T, Shinkai Y (2005) Histone methyltransferases G9a and GLP form heteromeric complexes and are both crucial for methylation of euchromatin at H3–K9. *Genes Dev* 19: 815 – 826

Takada Y, Naruse C, Costa Y, Shirakawa T, Tachibana M, Sharif J, Kezuka-Shiotani F, Kakiuchi D, Masumoto H, Shinkai Y-I *et al* (2011) HP1γ links histone methylation marks to meiotic synapsis in mice. *Development* 138: 4207 – 4217

Takahashi A, Imai Y, Yamakoshi K, Kuninaka S, Ohtani N, Yoshimoto S, Hori S, Tachibana M, Anderton E, Takeuchi T *et al* (2012) DNA damage signaling

triggers degradation of histone methyltransferases through APC/C Cdh1 in senescent cells. *Mol Cell* 45: 123 – 131

Thiru A, Nietlispach D, Mott HR, Okuwaki M, Lyon D, Nielsen PR, Hirshberg M, Verreault A, Murzina NV, Laue ED (2004) Structural basis of HP1/PXVXL motif peptide interactions and HP1 localisation to heterochromatin. *EMBO J* 23: 489 – 499

Timms RT, Tchasovnikarova IA, Antrobus R, Dougan G, Lehner PJ (2016) ATF7IP-mediated stabilization of the histone methyltransferase SETDB1 is essential for heterochromatin formation by the HUSH complex. *Cell Rep* 17: 653 – 659

Wysocka J, Swigut T, Xiao H, Milne TA, Kwon SY, Landry J, Kauer M, Tackett AJ, Chait BT, Badenhorst P *et al* (2006) A PHD finger of NURF couples histone H3 lysine 4 trimethylation with chromatin remodelling. *Nature* 442: 86 – 90

Yamamoto K, Sonoda M (2003) Self-interaction of heterochromatin protein 1 is required for direct binding to histone methyltransferase, SUV39H1. *Biochem Biophys Res Commun* 301: 287 – 292

Yamane K, Toumazou C, Tsukada Y-I, Erdjument-Bromage H, Tempst P, Wong J, Zhang YI (2006) JHDM2A, a JmjC-containing H3K9 demethylase, facilitates transcription activation by androgen receptor. *Cell* 125: 483 – 495

Zhang Y, Zhao L, Zhang J, Le R, Ji S, Chen C, Gao Y, Li D, Gao S, Fan H (2018) DCAF 13 promotes pluripotency by negatively regulating SUV 39H1 stability during early embryonic development. *EMBO J* 37: 1 – 15

